Analysis of Order-Statistic CFAR Threshold Estimators for Improved Ultrasonic Flaw Detection

Jafar Saniie, *Senior Member, IEEE*, and Daniel T. Nagle

Abstract—**An important problem in ultrasonic nondestructive evaluation (NDE) is the detection of flaw echoes in the presence of interfering and random echoes (i.e., clutter) associated with the microstructure of materials. In the pulse–echo method using broadband transducers, flaw detection can be improved by using optimal bandpass filtering to resolve flaw echoes surrounded by grain scatterers. Optimal bandpass filtering is achieved by examining spectral information of the flaw and grain echoes where frequency differences have been experimentally shown to be *predictable* in the Rayleigh scattering region. Using optimal frequency band information, flaw echoes can then be discriminated by applying adaptive thresholding techniques based on surrounding range cells. The paper presents order-statistic (OS) processors, ranked and trimmed mean (TM), to robustly estimate the threshold while censoring outliers. The design of these OS processors is accomplished analytically based on constant false-alarm rate (CFAR) detection. The OS-based CFAR detectors have been evaluated using experimental data and their performance is compared with the cell averaging (CA) method. It is shown that OS-CFAR and TM-CFAR processors can detect flaw echoes robustly with the CFAR of 10^{-4} where the range cell used for the threshold estimate contains outliers.**

I. Introduction

ULTRASONIC flaw detection in large-grained materials is difficult since grain scattering echoes interfere with and sometimes mask flaw echoes. Therefore, signal processing methods are essential to enhance the defect's echo leading to reliable detection. Fig. 1 shows an ultrasonic flaw detection system where the received ultrasonic signal is passed through a preprocessor for flaw-to-clutter ratio (FCR) enhancement, and is then compared to an adaptive threshold for constant false-alarm rate (CFAR) detection. Enhancement of the flaw-to-clutter ratio is accomplished by preprocessing the signal utilizing differences in the frequency and statistical information of the flaw and grain echoes using optimal frequency ranges and order-statistic processors. After preprocessing, the surrounding observations are used to create an adaptive threshold to allow for fluctuations in signal power. However, in certain instances, the existence of multiple flaws or high intensity noise information (i.e., outliers) requires a robust threshold estimate. Such threshold estimates can be obtained using order statistics that can censor extreme deviations from observations. Thus, the goal of this paper is twofold: 1) to develop and evaluate the effectiveness of preprocessing techniques for FCR enhancement, and 2) to analyze the design of CFAR detectors and their performance using experimental results.

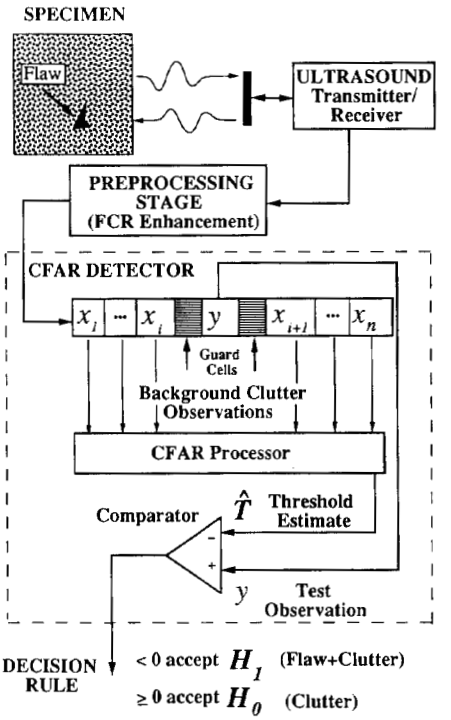

Fig. 1. Block diagram of ultrasonic CFAR flaw detection system.

In the Rayleigh scattering region, it has been shown [1]–[3] that grain scattering results in an upward shift in the expected frequency of the broadband ultrasonic signal. Although, this is not the case for flaw echoes since flaws are generally larger in size than the grain and behave like geometrical reflectors. In fact flaw echoes often display a downward shift in their expected frequency caused by the overall effect of attenuation. This downward frequency shift of the flaw is a productive attribute since the grain noise and flaw echoes are concurrently received and preprocessing methods can improve the flaw-to-clutter ratio. If the information-bearing frequency bands that

Manuscript received January 16, 1992; revised March 12, 1992; accepted March 16, 1992. This work was supported in part by SDIO/IST funds managed under contract S40000RB01 by the Office of Naval Research, and in part by Electric Power Research Institute contract RP 2405–22.

J. Saniie is with the Department of Electrical and Computer Engineering Illinois Institute of Technology, Chicago, IL 60616.

D. T. Nagle was with the Department of Electrical and Computer Engineering, Illinois Institute of Technology, Chicago, IL 60616 and is now with the Department of the Navy, Naval Underwater Systems Center, Newport, RI 02841.

IEEE Log Number 9201917.

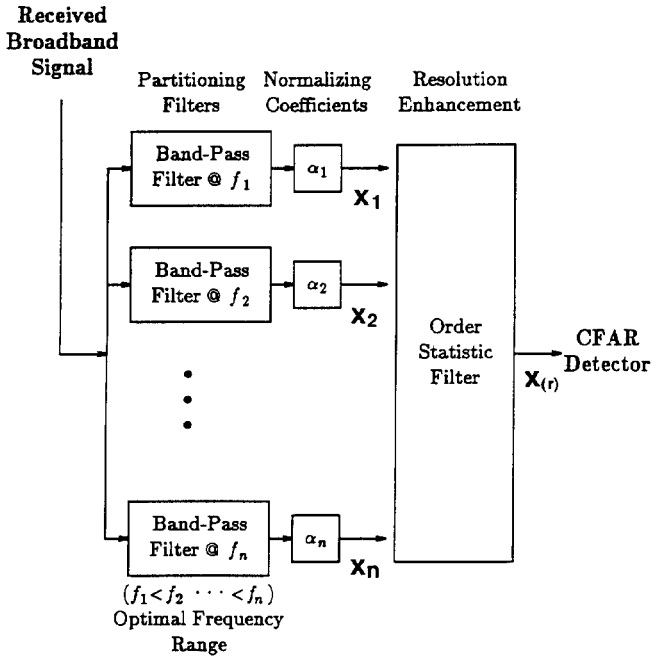

Fig. 2. Split-spectrum processing schematic.

are dependent on the specific characteristics of materials are known *a priori*, optimal bandpass filtering can be employed. However, if this information is unknown, other alternative flaw detection techniques that show less sensitivity to the environment are desirable.

Effective techniques for detecting targets in coherent noise are frequency agility or diversity that have been investigated in radar detection for several decades [4], [5] and more recently in ultrasound [6]–[9]. In an ultrasonic imaging system, a practical adaptation of these techniques has been examined and is referred to as split-spectrum processing (SSP). This method is based on transmitting a broadband signal into the media that, when received, is partitioned in several narrowband channels as shown in Fig. 2. The output of these channels is then processed to extract the flaw information in the channels with the highest flaw-to-clutter ratio.

Several split-spectrum processors such as maximization, median, minimization, averaging, and the quadratic detector [6]–[9] have been utilized in the past. An attractive procedure was shown to be minimization, specifically when in which the flaw is stationary and present in all of the channels [8], although, this requirement is not always satisfied in general [6]. If the flaw information is not present in some frequency bands, minimization will perform poorly and the median and maximization processors will perform more robustly [6]. In this paper, *optimal* bandpass filtering is applied to experimental data where the frequency characteristics of flaws and grains are predicted using *calibrated samples*. An additional degree of improvement in resolution is achieved by applying SSP when all selected narrow frequency bands comprise regions of high flaw-to-clutter ratios. The split spectrum technique provides a set of observations corresponding to different frequency bands that will decorrelate the microstructure noise. Furthermore, the performance of order-statistic processors in conjunction with the split-spectrum processing technique is analyzed in the context of FCR enhancement and resolution.

From the preprocessed data, the presence of the flaw is then *automatically* determined using CFAR detection. CFAR detectors have been utilized in radar systems where the clutter environment is partially unknown and/or has varying statistical properties (e.g., power). An effective method of compensating for changes in the clutter statistics is to use local threshold estimates from background clutter observations. In this paper, order-statistic (OS) and trimmed-mean (TM) CFAR detectors are considered for robust threshold estimation. The design of these CFAR detectors is modeled and compared with the experimental results when the background observations are contaminated with flaw information.

II. Frequency Analysis of Ultrasonic Signals

The exploration of the frequency content of ultrasonic backscattered signals can give spectral energy profiles corresponding to the grains and the larger geometric reflectors (i.e., defects). The energy loss of ultrasonic signals is caused by the microstructure of the propagating media through which scattering and absorption occurs. The model for the overall frequency-dependent attenuation coefficient $\alpha(f)$ is defined as

$$\alpha(f) = \alpha_a(f) + \alpha_s(f) \tag{1}$$

where $\alpha_s(f)$ is the scattering coefficient and $\alpha_a(f)$ is the absorption coefficient. The intensity of scattering is a nonexplicit function of the average grain diameter, ultrasonic wavelength, inherent anisotropic character of the individual grains, and the random orientation of the crystallites.

In the Rayleigh region (i.e., the wavelength is larger than the size of the grains), the scattering coefficient varies with the average volume of the grain and the fourth power of the wave frequency, while the absorption coefficient increases linearly with frequency [10]. The attenuation coefficient can be modeled as

$$\alpha(f) = a_1 f + a_2 \bar{D}^3 f^4 \tag{2}$$

where a_1 is the absorption constant, a_2, is the scattering constant, $\bar{D}$ is the expected grain diameter, and f is the transmitted frequency.

The composite effects of scattering and attenuation due to grains can be characterized in terms of transfer functions derived from the spectrums of measured signals. The transfer function associated with the scattering and attenuation of the grains is evaluated experimentally using two type 1018 steel specimens (i.e., Sample I and Sample II) where Sample I was not heat-treated and Sample II has been heat-treated at a temperature of 1900° for 4 h. The mean grain sizes of Samples I and II were found to be 14 and 50 μm (see Fig. 3), respectively. The backscattered ultrasonic signals and their spectrums are shown in Fig. 4 for different points in the steel blocks. Fig. 4(a) shows the front surface echo, $r_f(t)$, and spectrum, $|R_f(f)|$ of the flat front surface of the steel block positioned in the far field of the transducer. This front surface echo represents the response of the transducer impulse function, $U(f)$, the pulser, receiver amplifier, and the water

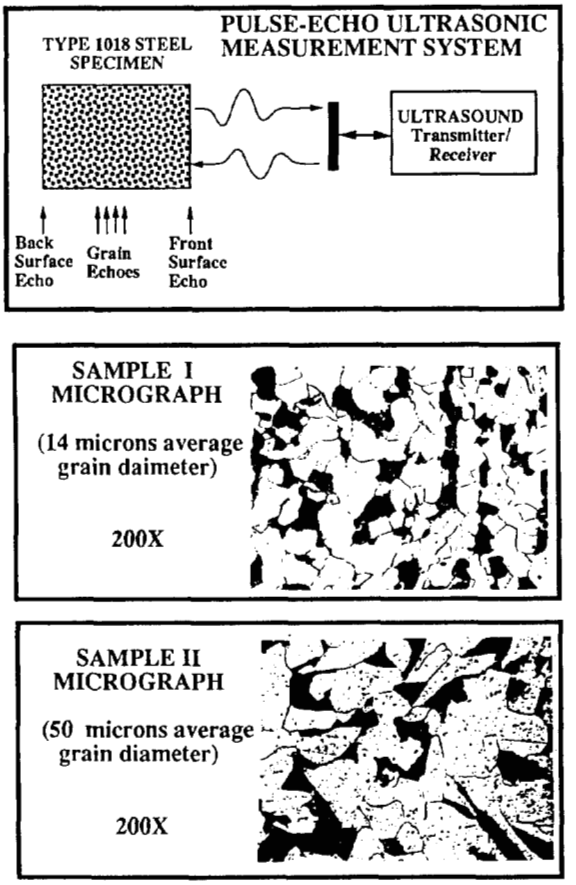

Fig. 3. Ultrasonic pulse–echo measurement schematic of steel blocks and the micrographs of the two steel specimens used for experimental studies.

propagation path. In the RF frequencies (1- to 15-MHz range), the characteristics of the pulser/receiver and water propagation path are frequency independent. Therefore, the received signal is proportional to the impulse response of the transducer:

$$|R_f(f)| \propto |U(f)|. \tag{3}$$

The spectrum, $|U(f)|$ can be modeled as a bandpass Gaussian-shaped spectrum centered approximately at 7 MHz with a 3-dB bandwidth of 3 MHz.

The effects of attenuation due to scattering and absorption of the propagating media are shown in Figs. 4(d) and (e) where a flat back surface echo travels 20 cm round trip into the steel samples I and II, respectively. The spectrum of the received signal, $R(f)$, can be modeled as

$$|R_b(f)| \propto |A(f)||U(f)| \tag{4}$$

where $A(f)$ is the transfer function corresponding to the attenuation characteristics of the signal propagation path. In Fig. 5(a), a heuristic evaluation of $|A(f)|$ is given by the ratio of the spectrums of the previously measured signals $|R_b(f)|/|R_f(f)|$. It can be seen that there is a definite shift or emphasis of the lower frequencies. This indicates that echoes associated with flaws significantly greater in size than the wavelength have dominant energy in lower frequencies.

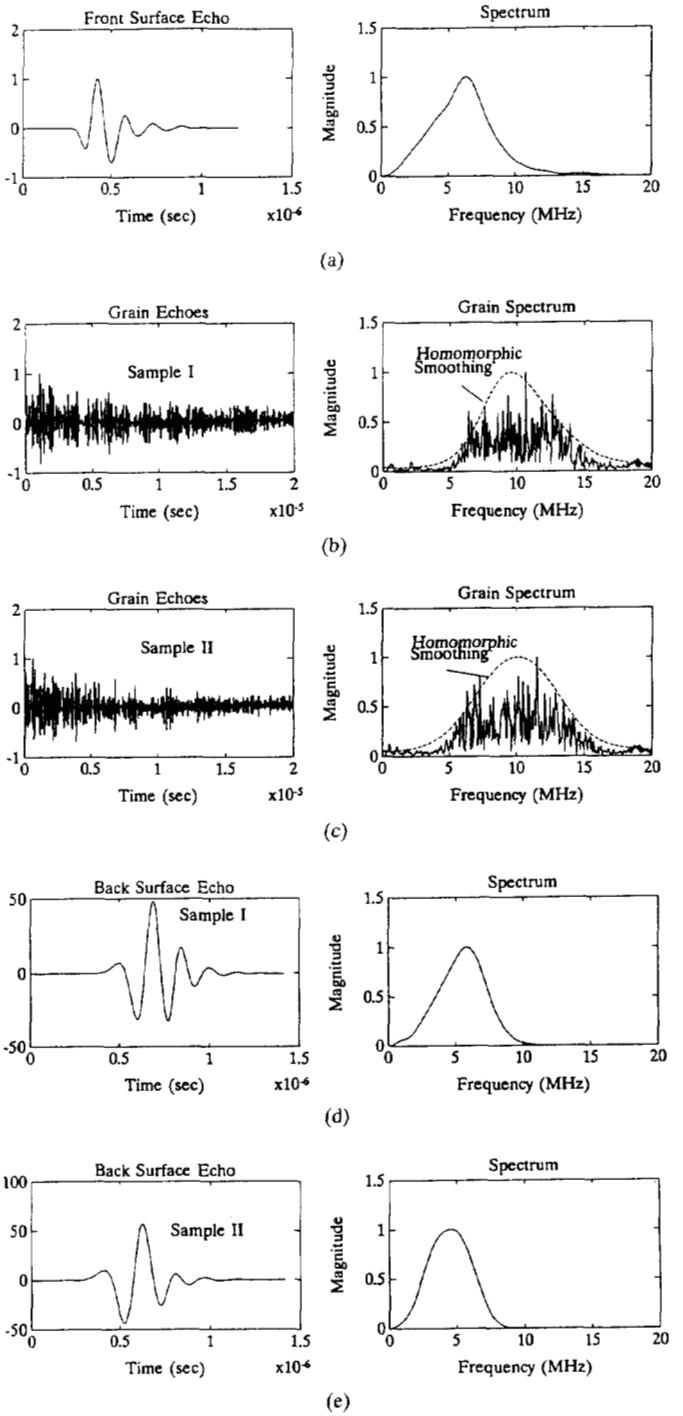

Fig. 4. Ultrasonic measurements and corresponding spectrums at different points (see Fig. 3) in the steel samples I and II with grain sizes of 14 μm and 50 μm, respectively. (a) A front surface echo (Sample I). (b) Grain echoes of Sample I. (c) Grain echoes of Sample II. (d) Back surface echo of Sample I. (e) Back surface echo of Sample II.

The spectrum of the signal received from grains alone is shown in Figs. 4(b) and (c), which can be modeled as

$$|R_g(f)| \propto |A(f)||S(f)||U(f)||G(f)| \tag{5}$$

where $|A(f)|$ is defined in (4), $|S(f)|$ is the frequency-dependent scattering function, and $|G(f)|$ is a frequency modulation function due to the sum of small scatterers with random orientations and phases [2]. The function $G(f)$ causes

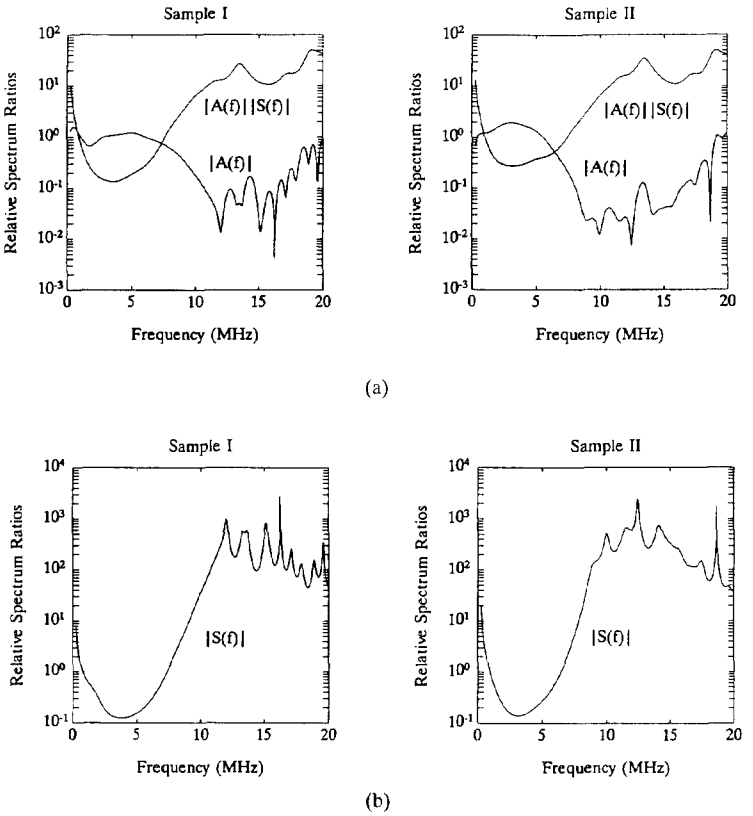

Fig. 5. Scattering and attenuation transfer functions of ultrasonic measurements, where (a) shows $|A(f)|$ (i.e., $|R_b|/|R_f(f)|$) and $|A(f)||S(f)|$ (i.e., $|\tilde{R}_g(f)|/|R_f(f)|$) for Samples I and II, and (b) shows $|S(f)|$ (i.e., $|\tilde{R}_g(f)|/|R_b(f)|$) for Samples I and II.

sporadic cancellations of frequency components and consequently results in the noisy spectrum shown in Figs. 4(b) and (c). To eliminate the effect of $G(f)$, homomorphic spectral smoothing techniques [2] are applied to measured grain signals in which the resulting smooth spectrum, $\tilde{R}_g(f) \propto |A(f)||S(f)||U(f)|$, is shown in Figs. 4(b) and (c) (dashed line) using a 28μs (approximately equivalent to the duration of a single echo governed by the characteristic of the transducer) shortpass lifter. Note that this duration for the shortpass lifter is chosen to provide sufficient smoothing [2]. The scattering function, $S(f)$, can be found by the ratios of the spectrums of the grain echoes ((5)) and the back surface echo ((4)), $\tilde{R}_g(f)/R_b(f)$, which is displayed in Fig. 5(b) for steel samples I and II. These results indicate that grain scattering causes the lower frequencies to become poorly backscattered (i.e., attenuated) resulting in an upward shift in the expected frequency of the grain spectrum. Thus, in order to take advantage of this property in flaw detection, frequencies where the grain scattering is minimal should be emphasized in order to maximize the flaw-to-clutter ratio.

In the Rayleigh region (i.e., wavelength of signal is greater than the grain diameter), the scattering and attenuation results of both steel samples (see Fig. 5(b)), in spite of significant differences in their grain sizes, show very similar frequency responses. Both flaw and grain echoes display predictable frequency dynamics associated with the physical properties of the steel sample. These results also indicate the frequencies where high flaw-to-clutter ratios exist and can be utilized in the preprocessing stage of the block diagram of Fig. 2. These characteristics are advantageous and lead to obtaining an optimal frequency range containing high flaw-to-clutter ratios for the SSP of the preprocessing stage.

III. Optimized Split Spectrum Processing

The disparity in the energy of lower frequencies of the grains and flaws allows bandpass filtering techniques to extract the flaw information in the preprocessing stage of Fig. 1. However, additional improvements in flaw-to-clutter ratio and resolution can be obtained through SSP techniques that focus on the statistical information in the frequency region of high flaw-to-clutter ratios. Thus, this section includes an outline of SSP techniques and presents the optimal performance that can be obtained using experimental measurements. Split spectrum processing entails transmitting a broadband signal into a media and partitioning the received signal into several narrowbands as shown in Fig. 2. The observations from the output of n channels are normalized with respect to the power (i.e., the output of all channels has the same power), $\alpha_i, i = 1, 2, \cdots, n$, and passed to an order-statistic processor. From here, the SSP output is passed to the CFAR detector for decision making as shown in Fig. 1.

It is critical to choose the parameters of the SSP appropriately in order to effectively enhance the flaw-to-clutter ratio [3], [7], [8], [11], [12]. The frequencies of the channels must reside within the information-bearing frequency range of the received signal, in particular, 2.5–5 MHz as shown in Fig. 5. Also, the bandwidth of the channels must be large enough

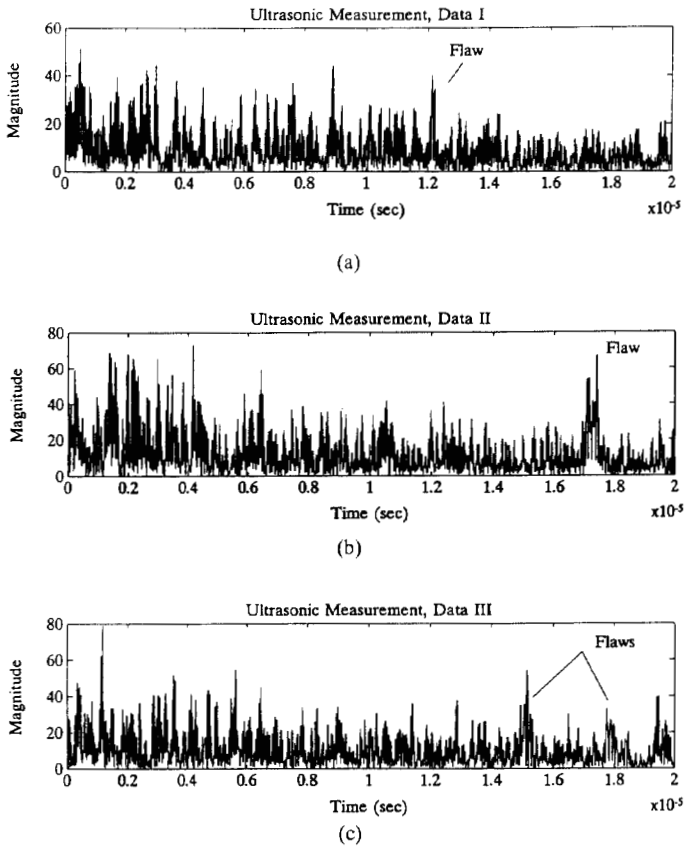

Fig. 6. Experimental ultrasonic flaw measurements, where (a) has a single flaw reflector, (b) three closely spaced unresolvable flaws, and (c) two spatially separated flaws.

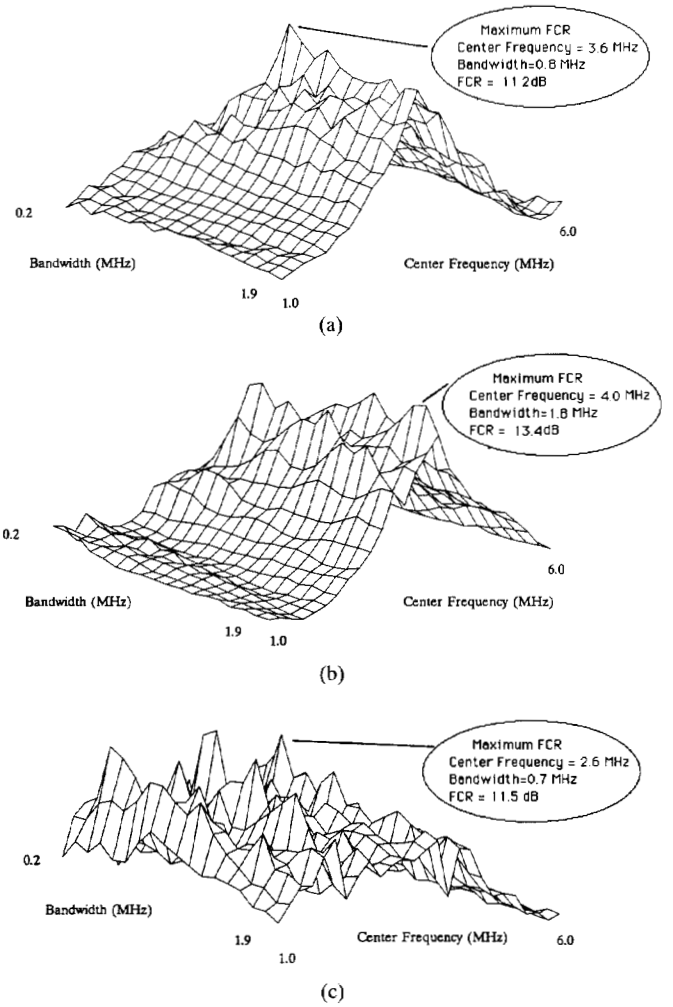

Fig. 7. Flaw-to-clutter ratio profiles of ideal bandpass (rectangular window) filtering with various center frequencies and bandwidths using (a) Data I (maximum FCR enhancement at 11.2 dB) and (b) Data II (maximum FCR enhancement at 13.4 dB), and (c) Data III (maximum FCR enhancement at 11.5 dB).

(0.5–1.0 MHz) to maintain the resolution integrity of the echoes. These constraints limit the number of observations attainable without excessive frequency overlap between bands. Correlation is not as critical as choosing frequency range with strong flaw information. Thus, typical frequency steps between channels will be 0.2–0.5 MHz.

To evaluate the importance of the optimal frequency range, three different experimental signals (shown in Fig. 6 and referred to as Data I, Data II and Data III) containing flaw echo with comparable amplitude to the clutter intensity (i.e., zero dB flaw-to-clutter ratio) are used. Fig. 7 shows the flaw-to-clutter ratio profiles for various ideal bandpass filters in terms of center frequency and bandwidth applied to Data I, II, and III. In Fig. 7(a), the Data I set from Sample I indicates that the frequencies near 3.5 MHz will give the best performance when bandwidths are 0.8 MHz or larger. Larger bandwidths offer robust performance for flaw detection since they will maintain the flaw information for shifts in different channels and also reduce the correlation of grain noise between channels. The flaw signal in Fig. 6(b), Data II, from Sample II, has a similar frequency profile (see Fig. 7(b)) as with Sample I. Comparisons of results shown in Figs. 7(a) and (b) indicates that the frequency differences due to grain size can be considered insubstantial enough to significantly alter the SSP optimal parameters. Therefore, using a typical specimen as the calibration tool for optimal frequency range is quite reliable.

The case for Data III from Sample II in Fig. 6(c) indicates that, for certain frequencies bands, interaction between the two flaw echoes and the grain echoes (shown in the FCR profile of Fig. 7(c)) have more fluctuations yet indicate similar conclusions (i.e., the FCR is low and unacceptable when the center frequency is beyond 6 MHz, and the FCR is relatively high when the center frequency is around 3.5 MHz and the bandwidth is about 0.8 MHz) as previously. The importance of this conclusion can be seen more clearly where five channels are used in the frequency range of 3–5 MHz (see Fig. 8) and the SSP output signals are shown in Fig. 9(a). As expected, each channel contains high flaw energy that is then fed to the order-statistic filter (see Fig. 2) to improve echo resolution and the flaw-to-clutter ratio.

The next step is to use the partially uncorrelated observations and make use of statistical differences in the channels (i.e., corresponding to random phase information in the received grain echoes) to improve the flaw-to-clutter ratio and resolution of the received echoes. The OS filter is shown in earlier work to be a quantile estimator [13] of the input density function that describes a specific point on the probability distribution function. The performance of the detector can be

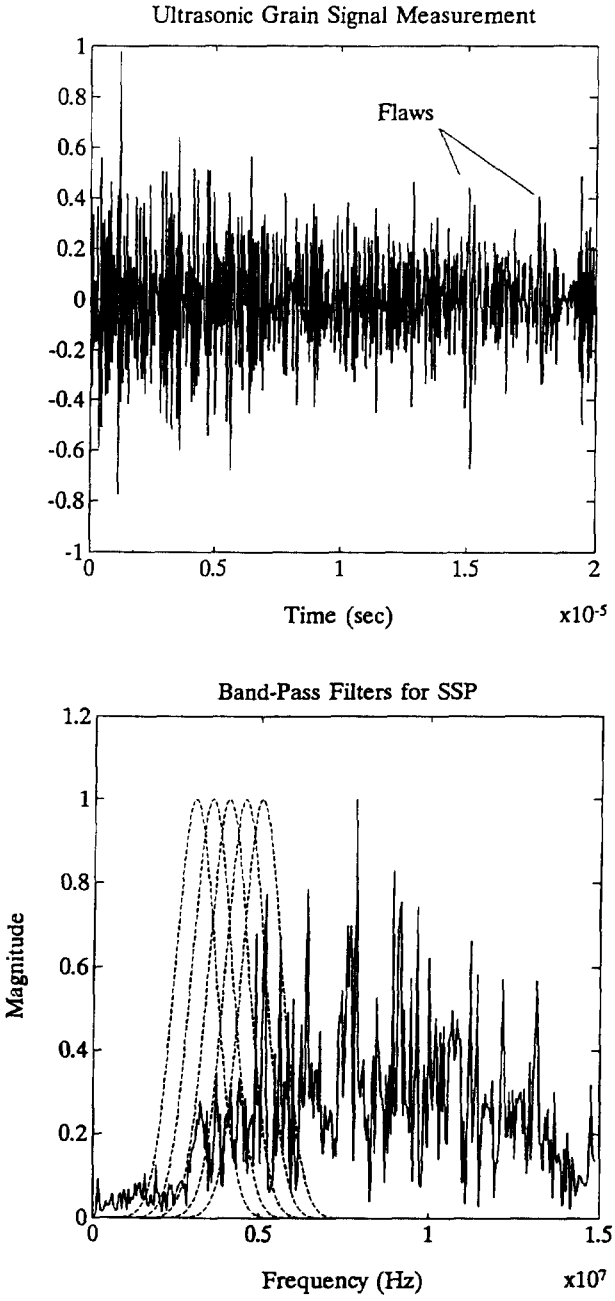

Fig. 8. Data III experimental signal and spectrum with five SSP filters used in the high flaw-energy frequency range.

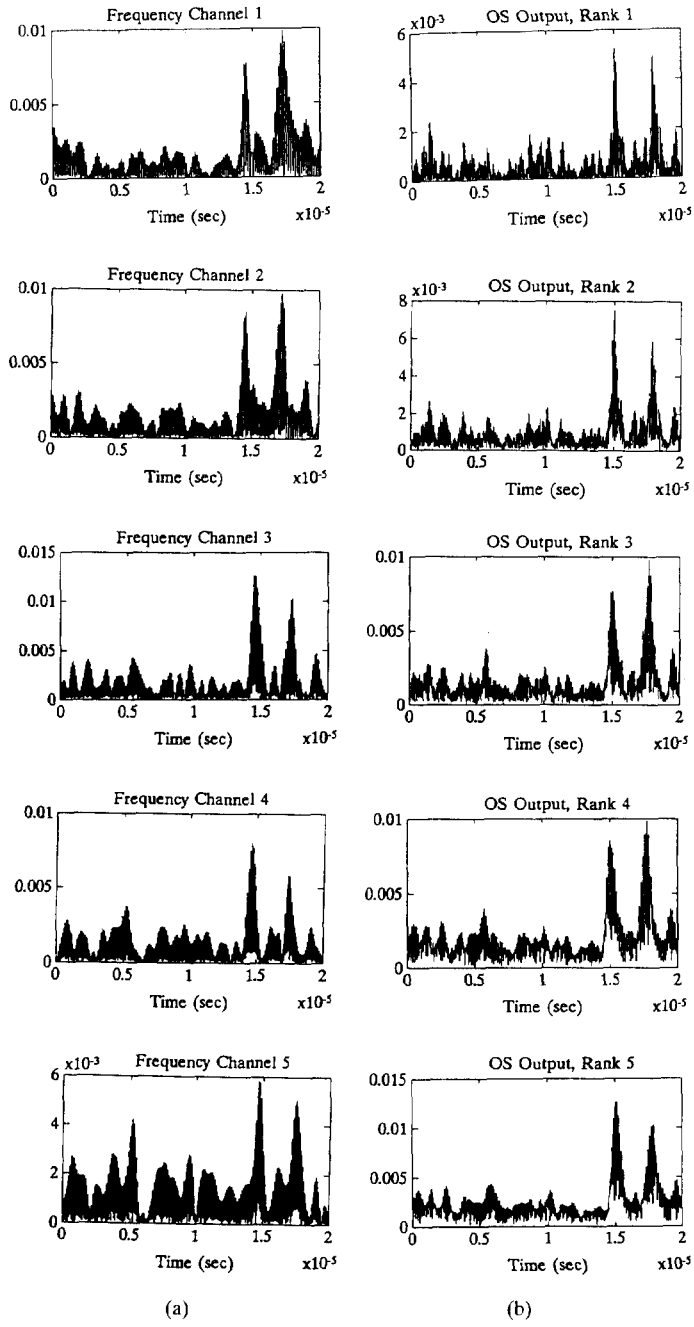

Fig. 9. SSP channels and respective OS outputs with five bandpass filters of 1-MHz bandwidth equally spaced between 3 and 5 MHz using Data III.

improved by choosing the position of the estimate where there are large statistical differences between the two hypotheses (flaw present, H_1, or not present, H_0).

The OS filter ranks a set of n input values corresponding to simultaneously sampled values of the n channels of the SSP output: $(x_1, x_2, x_3, \cdots x_n)$,

$$x_{(1)} \leq x_{(2)} \leq x_{(3)} \leq \cdots \leq x_{(n)} \tag{6}$$

where a given order or rank, r is chosen and $x_{(r)}$ is passed to the output. This processor is the median filter when $r = (n+1)/2$ (for odd n), the maximum filter when $r = n$ and the minimum filter when $r = 1$.

An important step for optimizing the OS filter involves finding the relationship between the input and output statistical behavior of the data. Assuming the input observations, x, are independent and identically distributed with distribution $F_X(x)$, the order statistic is known to be a consistent and asymptotically unbiased estimator of the quantile:

$$\lim_{\substack{n\to\infty \\ r\to\infty}} E\left[X_{(r)}\right] = F_X^{-1}(u_r) \tag{7}$$

where $u_r = (r-1)/(n-1)$ is a fixed constant, and $E[X_{(r)}]$ is the expected value for the output of OS filter. In the aforementioned limit both r and n approach infinity but u_r remains a finite ratio of r and n. For infinite n, the OS filter is an unbiased estimator. With finite observations, n, the estimate

will have some dispersion about the quantile value, u_r, that allows the values of neighboring quantiles to influence the output [14]. It should be noted that the performance of the OS filter will generally improve with increasing observations n since the variance will decrease (i.e., the random nature of the grains echoes will be reduced). The lower-ranked order statistics have been shown in the past to give improvement in the resolution of echoes and the flaw-to-clutter ratio [6] provided all channels have significant flaw information. The performance of all the ranked outputs of the SSP with five channels is shown in Fig. 9(b) in which all ranks show moderate improvement in the flaw-to-clutter ratios. The lower ranked outputs show slightly better resolution that is attractive in imaging multiple flaws.

Optimal SSP has been applied to several signals with various types of flaws in steel samples. Three experimental flaw measurements from steel samples I, II, and III are shown in Fig. 6 where Data I has a single simulated flaw (flat bottom hole), Data II has a complex flaw constituting three closely spaced (i.e., beyond the resolution of the system) flat-bottom holes, and Data III has two simulated flaws separated by 1.25 cm. The performance of the SSP with 11 channels of 1-MHz 3-dB bandwidth equally spaced between the frequency range of 3–5 MHz using minimum, median, and maximum order statistics is shown in Figs. 10–12 for Data I, II, and III, respectively. These figures show that the lower ranks provide improved resolution while maintaining the flaw-to-clutter level. Fig. 13 shows the SSP outputs with highest FCR of experimental signals using low-ranked order statistics. The next step is to utilize the optimized SSP output in reliable detection of the presence and position of flaw echoes where the background clutter/grain noise power fluctuates from region to region.

IV. Adaptive CFAR Threshold Estimators

In ultrasonic systems, the effect of interfering echoes from the microstructure can degrade the detection of a flaw within a particular range cell. When the clutter distribution in a measurement is unknown, the performance of the optimal (i.e., Neyman–Pearson fixed-threshold detector) detector deteriorates significantly, and the need arises for a nonparametric or CFAR detector that is designed to be insensitive to changes (e.g., power) in the density functions of the clutter.

In the past, CFAR detectors have been implemented using local observations in surrounding range cells to create local estimates of the threshold when these observations contain predominant clutter information [15]. A schematic of the CFAR detection system considered here is shown in Fig. 1. A single test observation, y, is classified to belong either to the null hypothesis (clutter), H_0, or the alternative hypothesis (flaw-plus-clutter), H_1, by using a local threshold, $\hat{T}$, estimated from a set of assumed clutter observations (belonging to H_0), $\boldsymbol{x} = \{x_1, x_2, \cdots, x_n\}$.

It has been shown that the cell averaging (CA) CFAR detector (i.e., $\hat{T} \propto \sum_{i=1}^{i=n} x_i$) performs optimally (offers maximum probability of detection) for homogeneous and

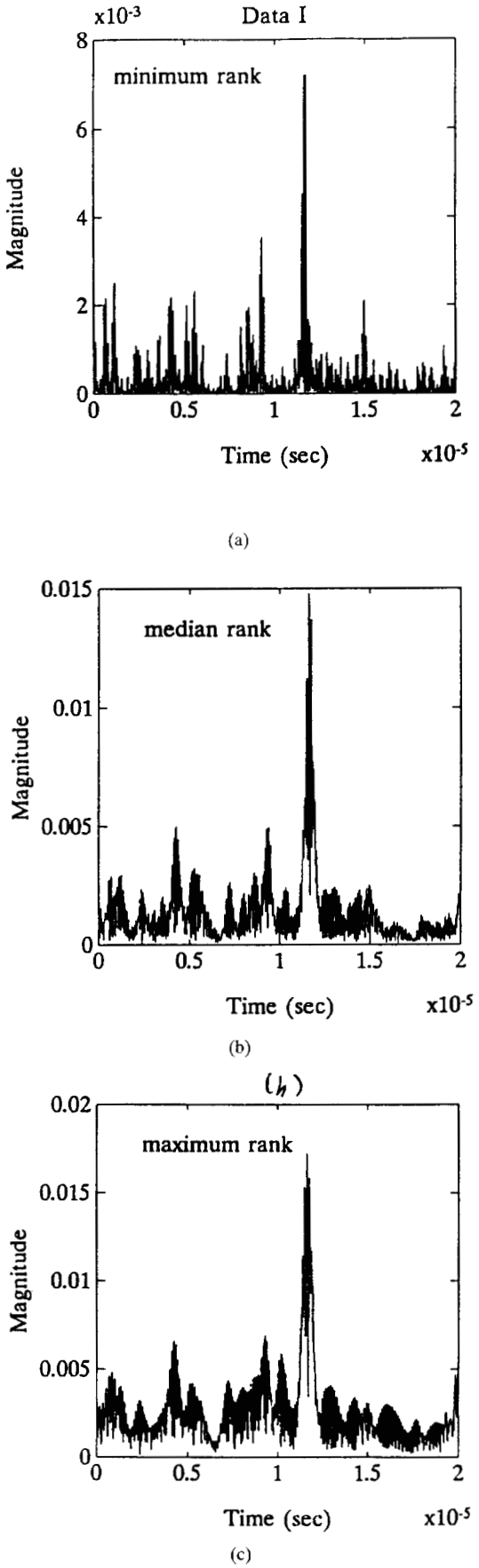

Fig. 10. SSP results with 11 channels of 1-MHz bandwidth equally spaced between 3 and 5 MHz using the (a) minimum, (b) median, and (c) maximum OS outputs for Data I.

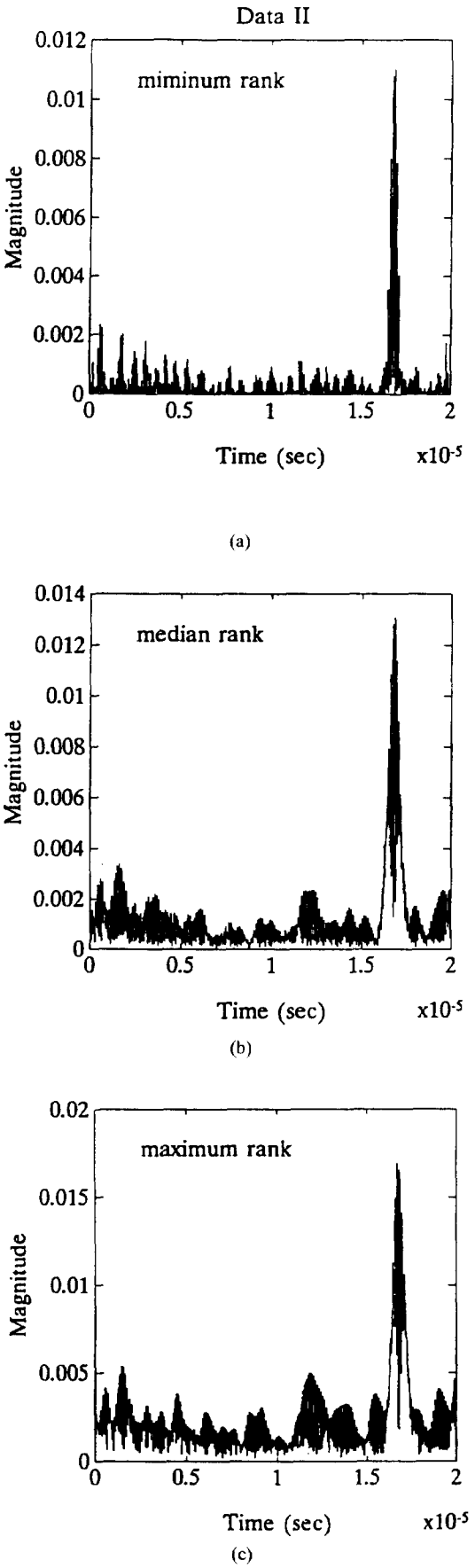

Fig. 11. SSP results with 11 channels of 1-MHz bandwidth equally spaced between 3 and 5 MHz using the (a) minimum, (b) median, and (c) maximum OS outputs for Data II.

exponentially distributed clutter observations:

$$F_0(x) = 1 - \exp[-x/\mu] \tag{8}$$

where $F_0(\cdot)$ is the clutter distribution and μ is the unknown scale parameter (i.e., related to the clutter power). The CA-CFAR detector is based on an application of the *invariance principle* [16]–[18] since the threshold estimator is a sufficient and complete estimator of the scale parameter μ. However, the performance of this optimized detector can significantly deteriorate when the assumption of homogeneous observations is violated (e.g., the introduction of flaw information and/or spurious noise). Thus, alternate methods that censor undesirable information (outliers) from the threshold estimate are required that will make the detector perform robustly.

The performance of the CFAR detector depends on the validity of assumed clutter observations, $\boldsymbol{x}$. Potential flaw information contained in the surrounding cells of $\boldsymbol{x}$ will generally degrade the probability of detection while maintaining the CFAR constraint. However, CFAR performance may be degraded by sharp transitions in the grain signal power (due to boundaries of materials) that is dependent on the size of clutter window, n. Taking these two scenarios into consideration, an intuitive solution can be obtained by censoring the clutter observations from large deviations (i.e., outliers) that would lessen the effects of the outliers, and consequently, improve the detector's performance. The censoring of data can be accomplished by using *order statistics*. This deviates from the application of order statistics in the SSP where the goal was to emphasize strong statistical differences in conjunction with improving the resolution through nonlinear signal processing techniques. In recent studies, censoring techniques have been implemented using OS-CFAR detectors [19] and TM-CFAR detectors [20] for radar applications. Utilizing the two estimates for required censoring needs, the OS- and TM-CFAR threshold estimates can be designed robustly resulting in improved detection for heterogeneous background observations.

The ideal CFAR threshold, T, for the one-sample test is given by

$$T = F_0^{-1}(1 - \alpha) \tag{9}$$

where $F_0^{-1}(\cdot)$ is the inverse distribution function for the null hypothesis (i.e., grain echoes or clutter) and the constant α is the probability of false alarm of the detector. Since $F_0^{-1}(\cdot)$ is not completely known *a priori*, the null observations, $\boldsymbol{x}$, are used to estimate the threshold, $\hat{T}$, as shown in Fig. 1.

The probability of false alarm for the CFAR detector, P_{FA} is given by

$$P_{FA} = P(Y > \hat{T} \mid H_0) \tag{10}$$

where Y is the random variable corresponding to the test observation with a distribution function $F_0(x)$ and a density function $f_0(x)$ under the null hypothesis H_0. Note that $\hat{T}$ is a

random variable with a distribution function $F_{\hat{T}}(\tau)$, a density function $f_{\hat{T}}(\tau)$, and observed values of $\hat{T}$ denoted by τ. P_{FA} can be expressed as

$$P_{FA} = \int_0^\infty [1 - F_0(\tau)] f_{\hat{T}}(\tau)\, d\tau \tag{11}$$

This expression shows the effect of the density function of the threshold estimate, $f_{\hat{T}}(\tau)$ on P_{FA}. If the threshold estimate is asymptotically unbiased and consistent, $f_{\hat{T}}(\tau)$ should converge to a delta function, $\delta(\tau - F_0^{-1}(1-\alpha))$, as n approaches infinity. However, for finite samples there will generally be spreading about the actual threshold value T governed by $f_{\hat{T}}(\tau)$. In order to satisfy the CFAR constraint described by (9), the threshold estimate must be adjusted, resulting generally in a biased estimate that can lower the probability of detection.

The threshold estimate for the CA-CFAR detector is given here:

$$\hat{T} = \theta \sum_{i=1}^{n} x_i \tag{12}$$

where θ is the scaling parameter, determined from the probability of false alarm relationship of (11).

The censored TM-CFAR threshold estimate corresponds to

$$\hat{T} = \theta \sum_{i=r+1}^{n-s} x_{(i)} \tag{13}$$

where r and s are the number of smallest and largest censored observations, respectively, and θ is the CFAR design parameter. This incorporates several order statistics that are combined linearly with equal weighting referred to as the TM-CFAR detector.

The OS-CFAR threshold is given by a scaled-order statistic:

$$\hat{T} = \theta x_{(i)} \tag{14}$$

as this is the special case of the TM-CFAR detector when $r = i - 1$ and $s = i + 1$.

The design parameter θ of CA-CFAR [15], OS-CFAR [19] and TM-CFAR [20] detectors for exponentially distributed observations can be found in a similar manner from (11). The P_{FA} for the CA-CFAR detector [15] is given by

$$P_{FA} = (1 + \theta)^{-n} \tag{15}$$

The P_{FA} for the TM-CFAR detector is given by [20]:

$$P_{FA} = \binom{n}{r}\binom{n-r}{s} \sum_{i=0}^{r} \frac{(-1)^{r-i}\binom{r}{i}}{(n-i)/(n-r-s)+\theta} \cdot \prod_{k=2}^{n-r-s} \left[\frac{n-r-k+1}{n-r-s-k+1} + \theta\right]^{-1}. \tag{16}$$

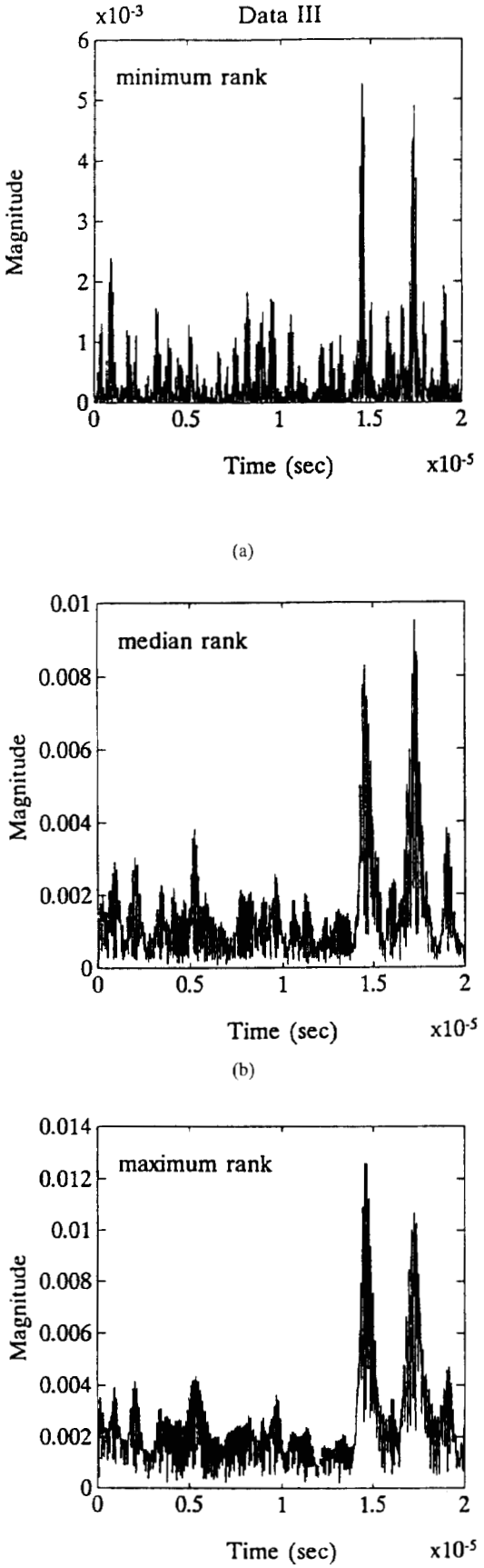

Fig. 12. SSP results with 11 channels of 1-MHz bandwidth equally spaced between 3 and 5 MHz using the (a) maximum, (b) median, and (c) minimum OS outputs for Data III.

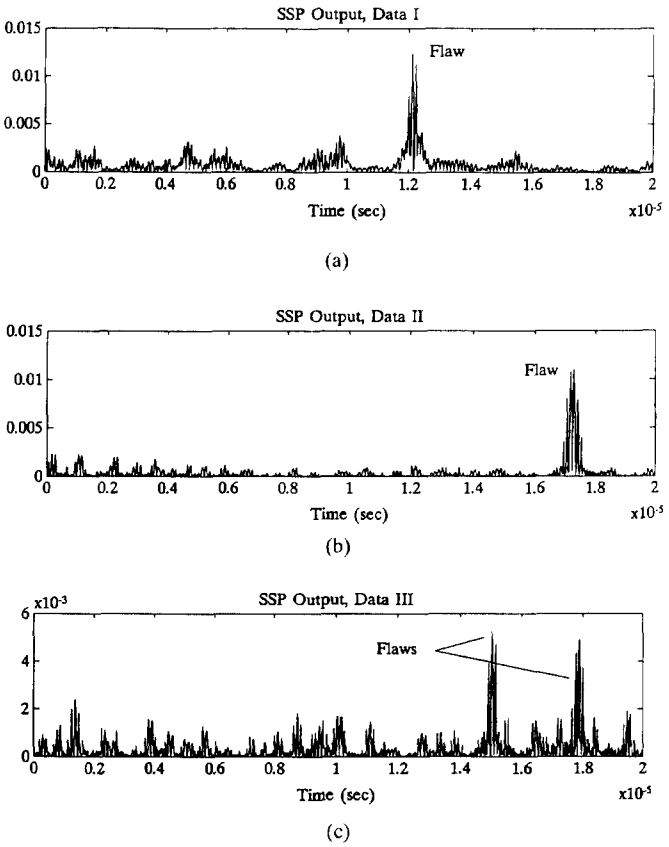

Fig. 13. Optimal SSP outputs for Data I, II, and III using ranks. (a) $r = 2$. (b) $r = 1$. (c) $r = 1$.

The P_{FA} for the OS-CFAR detector is given by [19]:

$$P_{FA} = i\binom{n}{i}\boldsymbol{B}(i, n-i+\theta+1) = \frac{n!\Gamma(n-i+\theta+1)}{(n-i)!\Gamma(n+\theta+1)} \tag{17}$$

where $\mathrm{B}(\cdot)$ and $\Gamma(\cdot)$ are Beta and Gamma functions [21], respectively. In this study, OS-CFAR and TM-CFAR detectors are implemented for different censoring scenarios their performance are examined and compared with CA-CFAR detector using experimental data.

V. CFAR Flaw Detection—Experimental Results

To implement the CFAR detector effectively, the parameters of the detector must be chosen in accordance with the resolution of the flaw echoes and the number of flaws present. For this study, experimental measurements and SSP outputs (Figs. 6 and 13, respectively) are used to illustrate different flaw scenarios where the preprocessed signals have comparable flaw-to-clutter ratios of approximately 11 dB. In Fig. 13(a), the signal shows a flaw from a single reflector. Fig. 13(b) shows a complex flaw echo with broader duration representing information relating to three closely spaced flat-bottom holes. An example with two resolvable flaws is shown in Fig. 13(c). These cases will be applied to the previously mentioned CFAR processors where the parameters are chosen to provide robust performance at equivalent levels of probability of false alarm ($P_{FA} = 10^{-4}$).

Since only one observation is used for testing (i.e., flaw information), the resolution of the flaw echoes requires guard cells to separate the samples containing concurrent flaw information from the threshold estimate of background clutter observations. The resolution of this system for the transducer center frequency of approximately 7 MHz (see Fig. 4(a)) and 3-dB bandwidth of 3 MHz and sampling rate of 100 MHz is approximately 25 samples. It is important to select a guard cell larger than the duration of a flaw echo to avoid contributing to the threshold estimate. The window size, n, for estimating the threshold must be large enough to cover adequate information related to clutter. In this study, n is equal to 128 data points, which covers approximately 12 periods of clutter signal (note that the sampling rate is 100 MHz and the expected center frequency for the clutter signal is about 10 MHz (see Figs. 4(b) and (c)). If n becomes too large, the threshold estimate becomes less adaptive to local clutter and the possiblity of including the outliers increases. if n becomes too small, then the threshold estimate will have a higher variance that leads to random performance.

An example of the performance of OS-CFAR, TM-CFAR, and CA-CFAR detectors for Data I is given in Fig. 14 for $n = 128$ and guard cells of 128 samples. This figure indicates that the guard cells maintain comparable clutter threshold levels for the region of the flaw, however, the presence of the two large peaks on either side of the flaw will prevent detection of other potential flaws in that region when multiple flaws occur. Results in this figure illustrates moderate (Fig. 14(a)) and extreme (Fig. 14(b)) censoring properties of the OS-CFAR and TM-CFAR detectors and how they reduce the effect of contaminating flaw information. It should be noted that the scaling factors derived from (15)–(17) assume that the clutter observations are exponentially distributed in which deviations in the probability of false alarm may exist. The performance of the OS-CFAR in this instance shows lower levels than the TM-CFAR threshold, however the TM-CFAR threshold has less variations, hence the TM-CFAR threshold would empirically perform with a lower incident of false alarm.

The CFAR performance using the same parameters as done previously using Data II, containing a composite flaw consisting of several unresolvable echoes, is shown in Fig. 15. This figure shows results similar to Data I. For Data III, where multiple flaws are present, Fig. 16 shows the case where CA-CFAR fails to detect flaw echoes due to contamination. Fig. 16(a) presents the moderate censoring case with guard cells of 444 where the flaw information is contaminating the threshold estimate of the neighboring flaw. In this example the OS reduces the effect of the outliers considerably producing thresholds comparable with the flaws where only the smaller flaw echo was not detected. The TM-CFAR threshold estimate shows the best performance in reducing the threshold bias and detects both flaws in the midst of high contamination. In the extreme censoring case with guard cells of 128 samples (see Fig. 16(b)), similar robust performance of the threshold estimate can be seen. In contrast to the performance of the

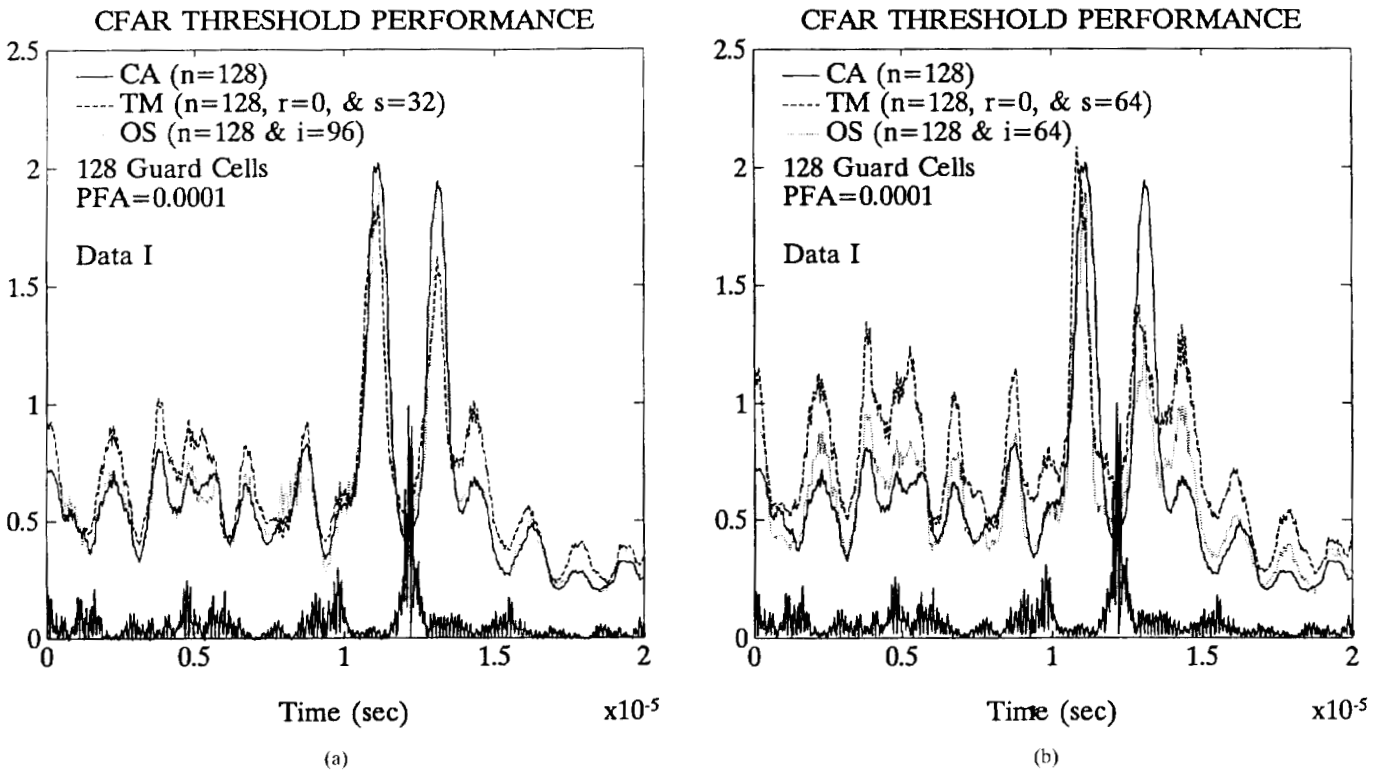

Fig. 14. Adaptive threshold performance for OS-, TM-, and CA-CFAR detectors for (a) moderate and (b) extreme censoring using Data I with $P_{FA} = 10^{-4}$.

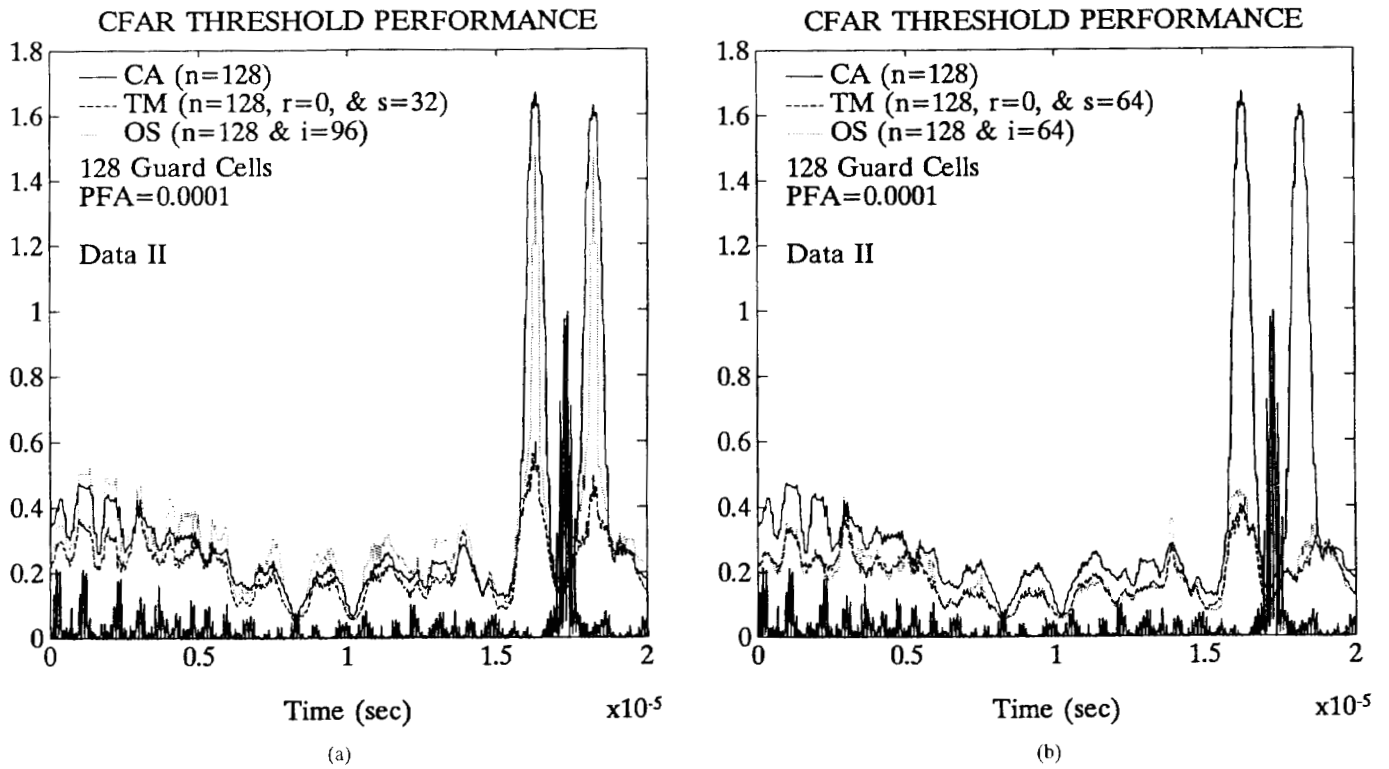

Fig. 15. Adaptive threshold performance for OS-, TM-, and CA-CFAR detectors for (a) moderate and (b) extreme censoring using Data II with $P_{FA} = 10^{-4}$.

CA-CFAR detector, both OS-CFAR and TM-CFAR thresholds robustly detect flaws in the presence of contaminating flaw information.

VI. Conclusion

In this paper, we have presented a theory and application of SSP parameters and CFAR detection in ultrasonic flaw

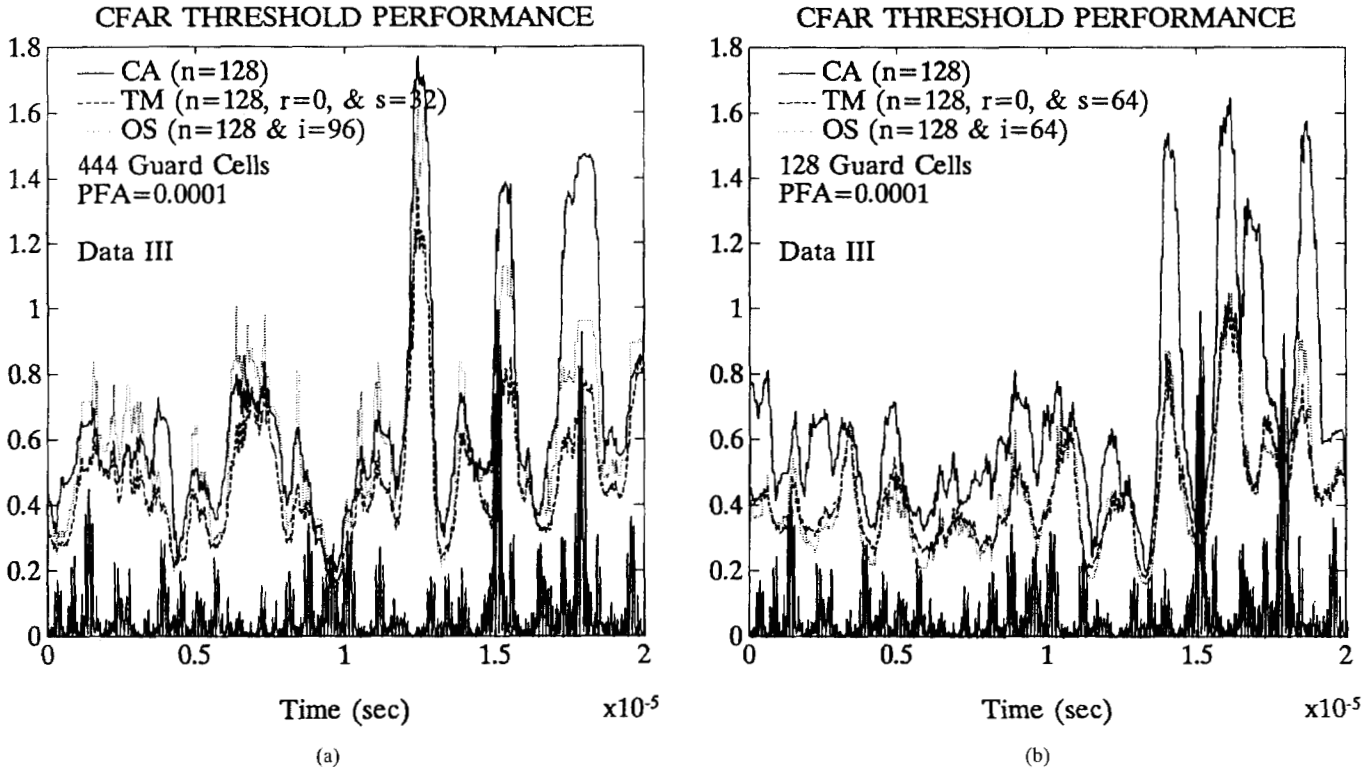

Fig. 16. Adaptive threshold performance for OS-, TM-, and CA-CFAR detectors for (a) moderate and (b) extreme censoring using Data III with $P_{FA} = 10^{-4}$.

detection. The theory suggests that the optimal SSP can be found upon the knowledge of the frequency ranges that can be determined through calibration. We have shown through experimental results that lower-ranked order statistics applied to the SSP perform well in terms of enhancing the flaw-to-clutter ratio and flaw resolution, although they require that all channels contain flaw information. Furthermore, the adaptive threshold has shown to maintain CFAR performance when the *a priori* knowledge of the distributions is incomplete. This paper introduces the application of CA-CFAR, OS-CFAR, and TM-CFAR threshold estimators for ultrasonic flaw detection in NDE application. These estimators have been applied to experimental data and results indicate that for the case of multiple targets, the OS-CFAR and TM-CFAR detectors show more robust performance than the CA-CFAR detector.

REFERENCES

[1] T. Wang, J. Saniie, and X. Jin, "Analysis of low order autoregressive models for ultrasonic grain signal characterization," *IEEE Trans. Ultrason., Ferroelec., Freq. Contr.*, vol. 38, pp. 116–124, Mar. 1991.

[2] J. Saniie, T. Wang, and N. M. Bilgutay, "Analysis of homomorphic processing for ultrasonic grain signal characterizations," *IEEE Trans. Ultrason., Ferroelec., Freq. Contr.*, pp. 365–375, May 1989.

[3] R. Murthy, N. Bilgutay, and J. Saniie, "Application of bandpass filtering in ultrasonic non-destructive testing," *Quantitative Nondestructive Evaluation of Materials (QNDE),* vol. 8, pp. 759–767, 1989.

[4] E. W. Beasley and H. R. Ward, "Quantitative analysis of sea clutter decorrelation with frequency agility," *IEEE Trans. Aerosp. Electron. Syst.*, vol. AES-4, pp. 468–473, May 1968.

[5] P. F. Guarguaglini, "A unified analysis of diversity radar systems," *IEEE Trans. Aerosp. Electron. Syst.*, vol. AES-4, pp. 418–420, Mar. 1968.

[6] J. Saniie, D. T. Nagle, and K. D. Donohue, "Analysis of order statistic filters applied to ultrasonic flaw detection using split-spectrum processing," *IEEE Trans. Ultrason., Ferroelec., Freq. Contr.*, vol. 38, pp. 133–140, Mar. 1991.

[7] N. M. Bilgutay and J. Saniie, "The effect of grain size on flaw visibility enhancement using split-spectrum processing," *Materials Evaluation,* vol. 42, pp. 808–814, May 1984.

[8] V. L. Newhouse, N. M. Bilgutay, J. Saniie, and E. S. Furgason, "Flaw-to-grain echo enhancement by split-spectrum processing," *Ultrasonics,* pp. 59–68, Mar. 1982.

[9] J. Saniie, T. Wang, and X. Jin, "Performance evaluation of frequency diverse Bayesian ultrasonic flaw detection," *J. Acoust. Soc. Amer.*, in press, Apr. 1992.

[10] E. P. Papadakis, "Ultrasonic attenuation caused by scattering in polycrystalline metals," *J. Acoust. Soc. Amer.*, vol. 37, pp. 703–710, 1965.

[11] P. Karpur, P. M. Shankar, J. L. Rose, and V. L. Newhouse, "Split spectrum processing: Optimizing the processing parameters using minimization," *Ultrason.*, vol. 25,pp. 204–208, July 1987.

[12] P. Karpur, P. M. Shankar, J. L. Rose and V. L. Newhouse, "Split spectrum processing: determination of the available bandwidth for spectral splitting," *Ultrason.*, vol. 26, pp. 204–209, July 1988.

[13] H. A. David, *Order Statistics.* New York: Wiley, 1981.

[14] J. Saniie, K. D. Donohue, and N. M. Bilgutay, "Order statistic filters as postdetection processors," *IEEE Trans. Acoustics, Speech, Signal Processing,* vol. 38, pp. 1722–1732, Oct. 1990.

[15] H. M. Finn, and R. S. Johnson, "Adaptive detection mode with threshold control of spatially sampled clutter-level estimates," *RCA Rev.*, vol. 30, pp. 414–465, Sept. 1968.

[16] E. L. Lehmann, *Testing Statistical Hypothesis.* New York: Wiley, 1959.

[17] L. L. Scharf, "Signal detection in Gaussian noise of unknown level: An invariance application," *IEEE Trans. Information Theory,* vol. IT-17, pp. 404–411, July 1971.

[18] P. G. Grieve, "The optimum constant false alarm probability detector for relatively coherent multichannel signals in Gaussian noise of unknown power," *IEEE Trans. Inform. Theory,* vol. IT-23, pp. 708–721, Nov. 1977.

[19] H. Rohling, "Radar CFAR thresholding in clutter and multiple target situations," *IEEE Trans. Aerosp. Electron. Syst.*, vol. 19, pp. 608–621, July 1983.

[20] P. P. Gandhi and S. A. Kassam, "Analysis of CFAR processors in nonhomogeneous background," *IEEE Trans. Aerosp. Electron. Syst.*, AES-24, pp. 427–445, 1988.

[21] M. Abramowitz, and I. A. Stegun, *Handbook of Mathematical Functions with Formulas, Graphs, and Mathematical Tables,* Nat. Bureau of Standards Appl. Math. Series, no. 55, Gov. Printing Office, Washington, DC, 1964.

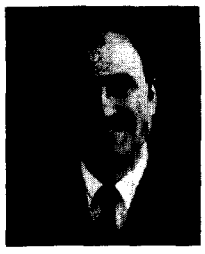

Jafar Saniie (S'80-M'81–SM'91) was born in Iran on March 21, 1952. He received the B.S. degree in electrical engineering from the University of Maryland in 1974. He received the M.S. degree in biomedical engineering in 1977 from Case Western Reserve University, Cleveland, OH, and the Ph.D. degree in electrical engineering in 1981 from Purdue University.

In 1981 he joined the Applies Physics Laboratory, University of Helsinki, Finland, to conduct research in photothermal and photoacoustic imaging. Since 1983, he has been with the Department of Electrical and Computer Engineering, Illinois Institute of Technology, Chicago, IL, where he is an Associate Professor and Director of the Ultrasonic Information Processing Laboratory. His current research activities include radar signal processing, estimation and detection, ultrasonic imaging, computer tomography, nondestructive testing, and digital hardware design.

Dr. Saniie is a Technical Committee Member of the IEEE Ultrasonics Symposium, and Editorial Advisory member of the *Nondestructive Testing and Evaluation Journal*. He is a member of Sigma Xi, Tau Beta Pi, Eta Kappa Nu, and has served as an IEEE Branch Counselor (1983–1990). He is the 1986 recipient of the outstanding IEEE Student Counselor Award.

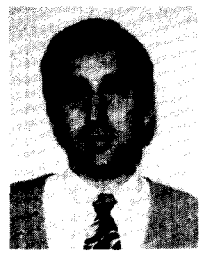

Daniel T. Nagle was born in Chicago, IL, on April 22, 1963. He received the B.S., M.S., and Ph.D. degrees in electrical engineering in 1985, 1987, and 1991, respectively from the Illinois Institute of Technology, Chicago, IL.

He is with the Department of the Navy at the the Naval Underwater Systems Center, Newport, Rhode Island. His research interests are in communication theory, signal and image processing, estimation and detection theory, and digital hardware design. During his graduate studies, he was supported by the Office of Naval Research and the Electric Power Research Institute.

Dr. Nagle is a member of Eta Kappa Nu.